Climate network percolation reveals the expansion and weakening of the tropical component under global warming

Jingfang Fan[a,b,c,1,2], Jun Meng[a,b,c,1], Yosef Ashkenazy[a], Shlomo Havlin[b], and Hans Joachim Schellnhuber[c,2]

[a]Department of Solar Energy and Environmental Physics, The Jacob Blaustein Institutes for Desert Research, Ben-Gurion University of the Negev, Midreshet Ben-Gurion 84990, Israel; [b]Department of Physics, Bar Ilan University, Ramat Gan 52900, Israel; and [c]Potsdam Institute for Climate Impact Research, 14412 Potsdam, Germany

Contributed by Hans Joachim Schellnhuber, October 19, 2018 (sent for review July 5, 2018; reviewed by Pinhas Alpert and Piet Van Mieghem)

Global climate warming poses a significant challenge to humanity; it is associated with, e.g., rising sea level and declining Arctic sea ice. Increasing extreme events are also considered to be a result of climate warming, and they may have widespread and diverse effects on health, agriculture, economics, and political conflicts. Still, the detection and quantification of climate change, both in observations and climate models, constitute a main focus of the scientific community. Here, we develop an approach based on network and percolation frameworks to study the impacts of climate changes in the past decades using historical models and reanalysis records, and we analyze the expected upcoming impacts using various future global warming scenarios. We find an abrupt transition during the evolution of the climate network, indicating a consistent poleward expansion of the largest cluster that corresponds to the tropical area, as well as the weakening of the strength of links in the tropic. This is found both in the reanalysis data and in the Coupled Model Intercomparison Project Phase 5 (CMIP5) 21st century climate change simulations. The analysis is based on high-resolution surface (2 m) air temperature field records. We discuss the underlying mechanism for the observed expansion of the tropical cluster and associate it with changes in atmospheric circulation represented by the weakening and expansion of the Hadley cell. Our framework can also be useful for forecasting the extent of the tropical cluster to detect its influence on different areas in response to global warming.

climate network | percolation | global warming | Hadley cell

The series of powerful Atlantic hurricanes that hammered the Americas, the "Lucifer" heat wave that stifled Europe, and the unusually dry June in Australia, all occurring in 2017, have been associated with the increased risks of extreme weather events (1). Indeed, recent strong evidence supports the claim that this increase in extreme events is directly related to global warming (2). Although some scientists question the significance of and the role played by human activity in global warming, the majority of the scientific community agrees that the warming is anthropogenic, due to elevated concentrations of heat-trapping (greenhouse) gases, especially triggered by the increased burning of fossil fuels and deforestation (3). Global climate warming could influence the nature of societies and the performance of economies (4–8) by impacts on global temperature, sea level, precipitation, ocean currents, and so on (9–12).

Network theory has demonstrated its potential as a useful tool for exploring the dynamical and structural properties of real-world systems from a wide variety of disciplines in physics, biology, and social science (13–19). Network approaches have been successfully implemented in climate sciences to construct "climate networks," in which the geographical locations are regarded as network nodes, and the level of similarity between the climate records of different grid points represents the network links (strength). Climate networks have been successfully used to analyze, model, and even predict climate phenomena (20–24). Percolation theory was found to be an effective tool for understanding the resilience of connected clusters to node breakdowns through topological and structural properties (25–27). The essence of the analysis is the identification of a system's different components and the connectivity between them. Percolation theory was applied to many natural and human-made systems (18, 25, 28–30). Here, we combine climate network and percolation theory approaches to develop a framework with which to study and quantify the dynamical structure of the global climate system. Our results suggest that an abrupt first-order percolation (phase) transition occurs during the evolution of the spatiotemporal climate networks. This evolution indicates the weakening and expansion of the giant component (tropical cluster) and is consistent with reported changes (expansion and weakening) of the tropical (Hadley) circulation.

Spatiotemporal Climate Networks

Similar to earlier studies (21, 23), we construct a climate network based on the near-surface (monthly mean), high-resolution (0.125°), air temperature of the ERA-Interim reanalysis data (31). (Details are discussed in *Data and Methods*.) We focus on the surface-temperature field since it probably is the most commonly discussed global-warming field; other variables, as well as other vertical layers, can be analyzed similarly to the way described below. Our evolving clustering process starts globally with $N = 1439 \times 2880$ isolate nodes. (The South and North Pole

Significance

Climate change could threaten our society through impacts on social, cultural, and natural resources. Here, we develop an approach based on percolation theory and climate network frameworks to detect and quantify the impacts of past and future climate change. Our method of analysis provides a perspective on the evolution of climate systems in response to global warming and can potentially be used for predicting the consequences of future climate changes. Furthermore, our study may also enrich and facilitate the understanding of discontinuous phase transitions.

Author contributions: J.F., J.M., Y.A., S.H., and H.J.S. designed research; J.F., J.M., and H.J.S. performed research; J.F., J.M., Y.A., and S.H. contributed new reagents/analytic tools; J.F., J.M., Y.A., S.H., and H.J.S. analyzed data; and J.F., J.M., Y.A., S.H., and H.J.S. wrote the paper.

Reviewers: P.A., School of Geosciences, Tel-Aviv University; and P.V.M., Delft University of Technology.

The authors declare no conflict of interest.

[1]J.F. and J.M. contributed equally to this work.

[2]To whom correspondence may be addressed. Email: jingfang@pik-potsdam.de or john@pik-potsdam.de.

This article contains supporting information online at www.pnas.org/lookup/suppl/doi:10.1073/pnas.1811068115/-/DCSupplemental.

Published online December 26, 2018.

grid points are eliminated.) We then embed the network into a 2D lattice where only nearest neighbor links are considered. The links are sorted in decreasing order of strength and then added one by one according to decreasing strength W (see Eq. **4** below); i.e., we first choose the link with the highest weight, then the second strongest link, and so on. More specifically, the nodes that are more similar (based on their temperature variations) are connected first. Existing clusters grow when a new link connects one cluster to another cluster (as small as a single node). We find that the climate network undergoes an abrupt and statistically significant phase transition, i.e., exhibiting a significant discontinuity in the order parameter G_1, the relative size of the largest cluster. Our results indicate that links with higher similarities tend to localize into a few large components (clusters of nodes) in the tropics and in the higher latitude regions (poles) of the Northern Hemisphere (NH) and Southern Hemisphere (SH). (We show the dynamical evolution of the climate networks in Movie S1.)

Fig. 1*A* shows the climate network component (cluster) structure in the globe map at the percolation threshold (just before the largest jump that is indicated by the orange arrow in Fig. 1*B*). We find that the network, just before this jump, is characterized by three major communities; the largest one is located in the tropical region (indicated by red color); the second and third largest are located in the high latitudes of the SH (indicated by blue color) and NH (indicated by green color). In the next step, a critical bond will connect and merge the tropical cluster with the SH cluster, resulting in a giant component. Fig. 1*B* depicts the relative size of the largest cluster (the order parameter), G_1, as a function of the bond/link occupation probability r in the evolution of the climate network. We find that G_1 exhibits an abrupt jump at the percolation threshold $r_c \approx 0.53$. The probability density function (PDF) of the weight $W_{i,j}$ of links is shown in Fig. 1*D*.

To study the significance of these results, we constructed the PDF of (temporally or spatially) reshuffled temperature records. In this way, either the memory within each record or the cross-correlations between the records are destroyed. We repeated the shuffling procedure 100 times and calculated their corresponding PDFs. The results, shown in Fig. 1 *B* and *D*, indicate that in contrast to the randomly shuffled case, where the transition is continuous, the giant component in our real climate network shows an abrupt change. The vertical line in Fig. 1*D* indicates the strength of the critical link W_c at the percolation threshold r_c. In addition, we find that W_c is also larger than the 95% confidence level of the randomly shuffled data. We find that the percolation threshold in the real network at $r \approx 0.53$ is larger than the expected 0.5 in the random (reshuffled) lattice and G_1 seems to increase almost "piece-wise" linear with r. The possible explanation is as follows: the transition for the shuffled (random) case span r values from a value that is slightly smaller than 0.5 to r value that is larger than 0.5—we conjecture that for infinitely long time series, the transition would have been more pronounced and narrower, converging to the theoretical transition value of 0.5. As for the piece-wise linear dependence of the data, as seen in Movie S1, links with higher similarities tend to localize into a few large components (clusters of nodes), in the tropics and in the higher latitude regions (poles) of the NH and SH. Thus, when two of these clusters join together,

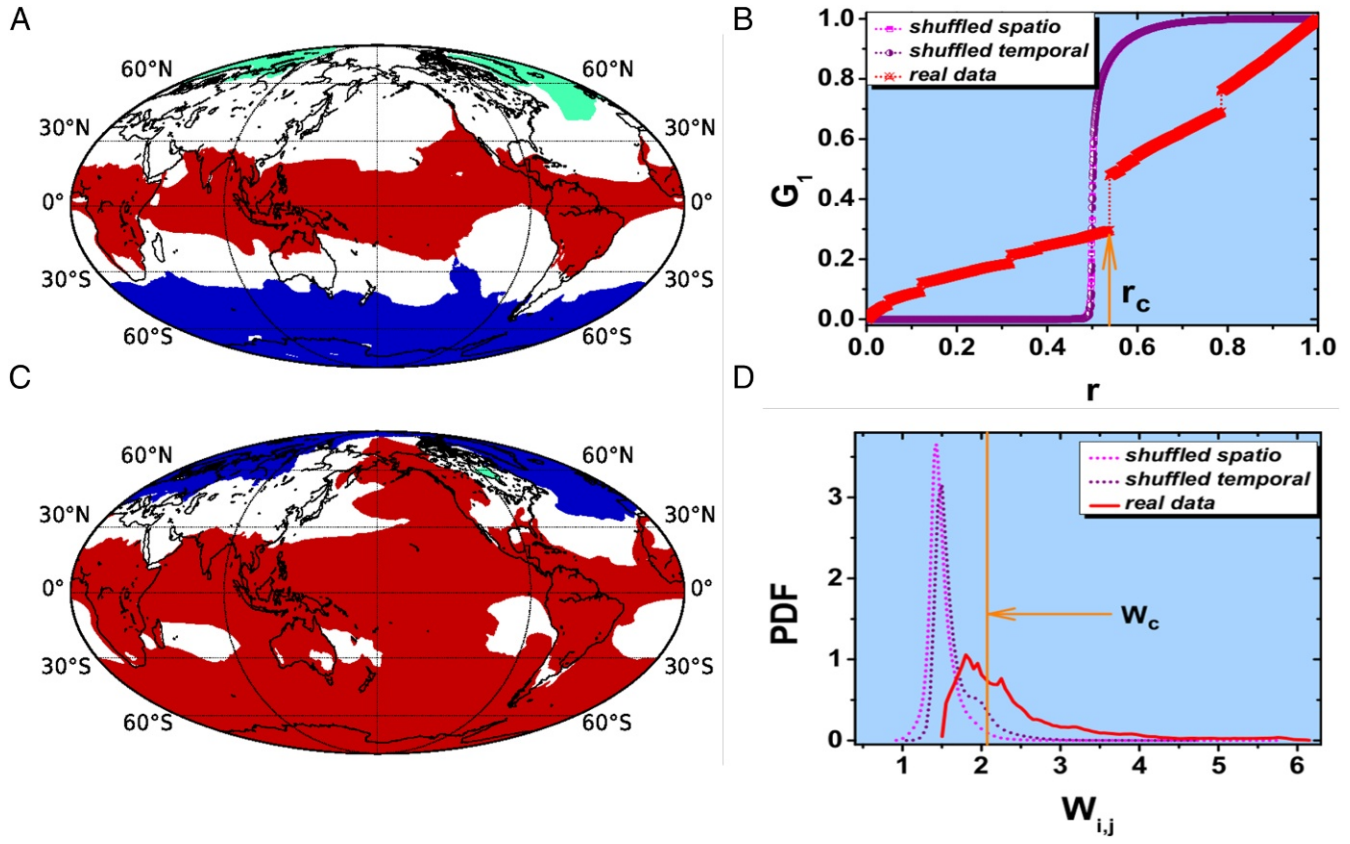

Fig. 1. Snapshots of the component structures of the climate network. (*A*) Just before the percolation threshold (the largest jump at $r \approx 0.53$). Different colors represent different clusters; the grid resolution is 0.125°. (*B*) The giant cluster relative size G_1 versus the fraction number of bonds/links, r, for real (red), spatially shuffled (blue), and temporally shuffled (purple) records. (*C*) Just before the formation of the spanning cluster (at the second largest jump at $r \approx 0.8$). (*D*) The PDF of the weight of links $W_{i,j}$ around the globe, in real (solid line) and shuffled (dashed lines) data. The vertical line (orange) indicates the strength of the critical link, W_c, at the percolation threshold $r_c \approx 0.53$; it is also higher than the 95% confidence level of the randomly shuffled links.

there is an abrupt jump in the curve—the linear like increase in between is due to the (linear) increase of very small neighboring clusters. For the continuous phase transition, there is no localized clustering mechanism of spatial structure, since links are added randomly.

During the growth of the climate network, we find, in Fig. 1*B*, that there are other smaller jumps. For example, the second largest jump occurs at $r \approx 0.8$, which is caused by the merging of the global cluster with the NH high-latitude cluster shown in blue in Fig. 1*C*.

To determine the temporal evolution of the size of the largest component G_c (just before the largest jump at r_c) and its intensity W_c (the weight of the critical link that leads to the largest transition; for more details on G_c and W_c, see *Data and Methods*), we construct a sequence of networks based on successive and nonoverlapping temporal windows with lengths of 60 mo (5 y) each. Fig. 2*A* depicts W_c as a function of time, indicating a significant decrease with time; G_c shown in Fig. 2*B*, however, exhibits an increasing trend with time. Specifically, by comparing the topological tropical component structures of the first and the last climate networks (shown in *SI Appendix*, Fig. S1), we find that the tropical cluster is expanding poleward. This weakening and poleward expansion of the tropical component may be associated with global warming, as discussed below. An alternative definition of the cluster intensity is $\langle W \rangle$, the average weight of links in the tropical cluster at the percolation threshold; this yields similar results (see *SI Appendix*, Fig. S2).

Next, we investigate the response of the tropical component to global warming using 21st century global warming experiments CMIP5 (32). We used the Representative Concentration Pathways 8.5 (RCP8.5) and 4.5 (RCP4.5) and Historical scenarios; the first two are future (21st century) climate simulations under the assumption of warming by 8.5 and 4.5 W/m^2, respectively. The results indicate a significant weakening and expansion of the tropical component for 26 out of 31 models in the RCP8.5 scenario. (Details are summarized in *SI Appendix*, Table S1.) In Fig. 2 *C* and *D*, we illustrate the changes of W_c and G_c with time, from 2006 to 2100 for one model, MIROC-ESM, under the RCP8.5 scenario. These W_c and G_c exhibit significant decreasing and increasing trends where the slope of the trends (i.e., the rate of change of W_c and G_c with time), ξ_W and ξ_G, can be used to quantify the trend of each model (see Eq. **7**). Fig. 3 *A*–*C* shows the results of ξ_W and ξ_G for all 31 models, for the RCP8.5, RCP4.5, and Historical scenarios. We find that most of the models [26/31 (RCP8.5), 17/20 (RCP4.5), 22/31 (Historical)] show a stable trend and are located in the same phase (i.e., $\xi_W < 0$ and $\xi_G > 0$). The details (label number and resolution) of the 31 models we used are summarized in *SI Appendix*, Table S1. Since the values (or the PDF) of W_{ij} strongly depend on three features: (*i*) datasets, (*ii*) the range of the time lags, and (*iii*) the length of the records, there is no high motivation to compare different datasets, lags, and records for the values of W_{ij}. We note that the values of ξ_G (ξ_W, ξ_{ϕ_H}) scales for future RCP4.5 and RCP8.5 are very different from the Historical values (in Fig. 3). This is since for the Historical data, we used only 25-y data, from 1980 to 2005 (due to the significant warming trend observed during this period), while for the RCP8.5 and RCP4.5 data, we used 95 y data, from 2006 to 2100.

Mechanism

To study a possible climatological origin of the aforementioned results—weakening and expansion of the tropical cluster—we consider now the atmospheric circulation, especially, the Hadley cell (HC), which plays a pivotal role in the earth's climate by transporting energy and heat poleward. The HC is a global scale tropical atmospheric circulation that features air rising near the Equator, flowing poleward at 10–15 km above the surface, descending in the subtropics, and then returning equator-ward near the surface. We conjecture that the tropical component of the climate network can be linked to the HC, since both of them

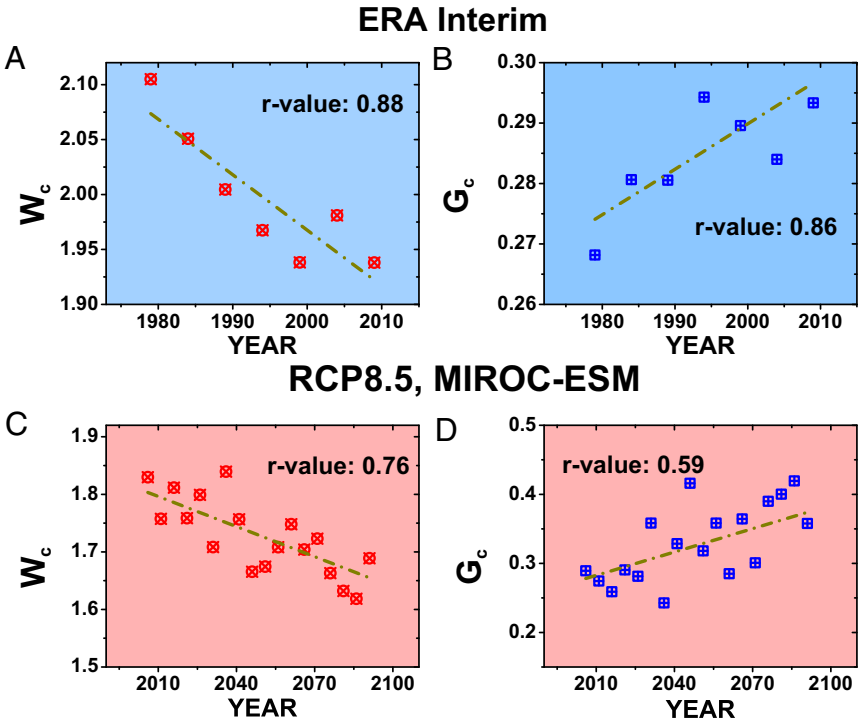

Fig. 2. Weakening and expansion of the tropical component for (*A* and *B*) the ERA-Interim reanalysis data and for (*C* and *D*) a CMIP5 model, MIROC-ESM, under the RCP8.5 global warming scenario. W_c is the weight of the critical link; G_c is the normalized size of the tropical component just below r_c, as shown in Fig. 1*A* with red color. Linear correlation coefficients (*r* values) are given in the panels.

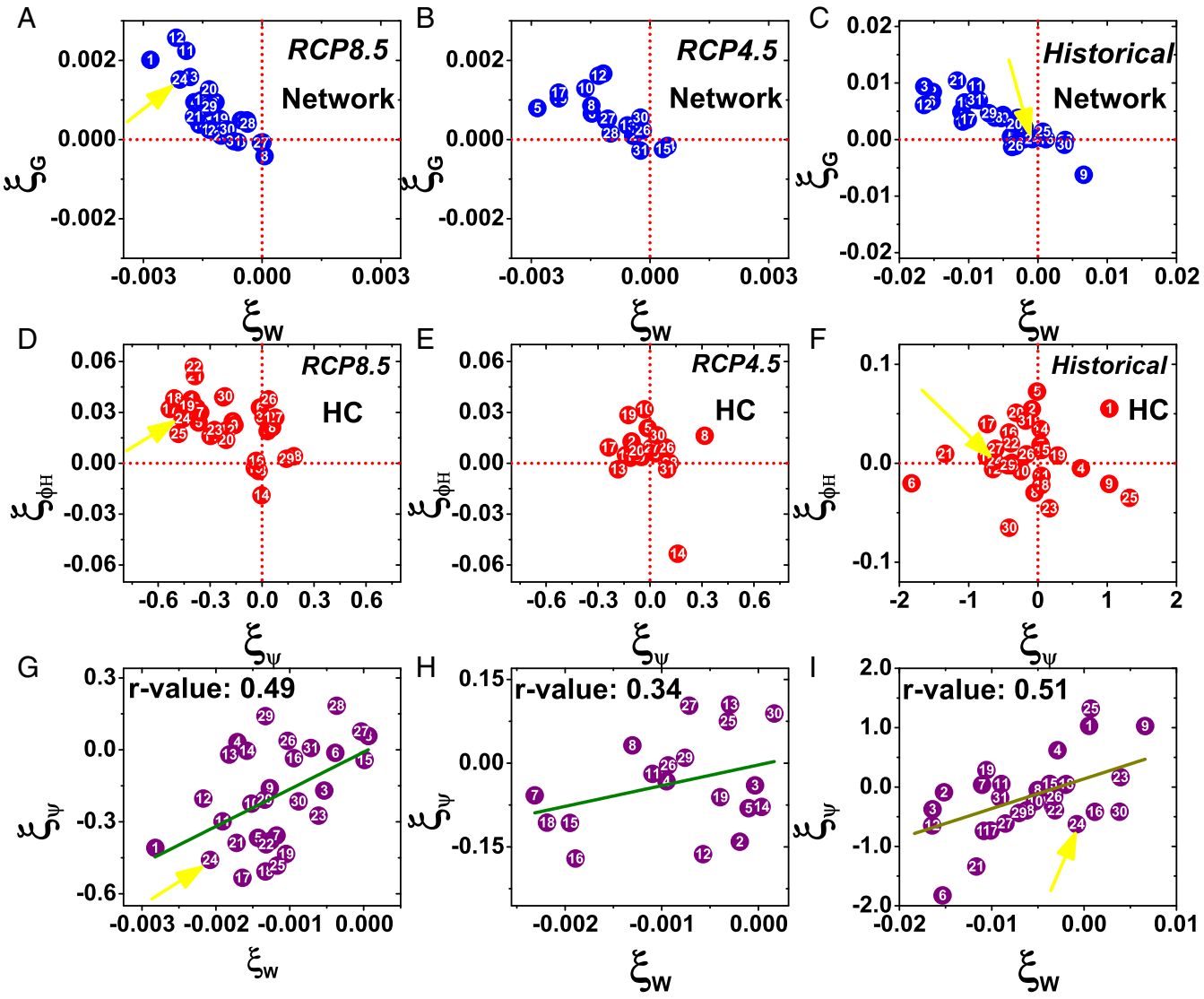

Fig. 3. Changes in the size of the giant component against changes in the intensity for the network tropical component and the HC. The scatter plots of the increasing (size) and decreasing (intensity) trends for the RCP8.5 scenario (*A* and *D*); RCP4.5 scenario (*B* and *E*); and Historical scenario (*C* and *F*). (*G–I*) Changes in the intensity of the HC against the network tropical component. Linear correlation coefficients (*r* value) are given in the different panels. We use the yellow arrows lines to indicate the location of MIROC-ESM. The numbers in the circles corresponding to the 31 models are summarized in *SI Appendix*, Table S1.

exhibit consistent weakening and poleward expansion under global warming. In other words, the poleward expansion and weakening of the HC under global warming scenarios are linked to the expansion and weakening of the network-based tropical cluster. Below, we present results that support this conjecture.

An analysis of satellite observations indicates a poleward expansion of the HC by $\sim 2^\circ$ latitude from 1979 to 2005 (33). The main mechanisms for changes in the HC and its relation to global warming have yet to be elucidated (34). A possible mechanism for the changes in the HC's and its relation to global warming has been proposed in ref. 35. Also, a possible mechanism for the changes in the HC's strength and its relation to global warming was developed in ref. 36. Both abovementioned observations and theories suggest a weakening and poleward expansion of the HC under global warming.

To find the relationship between the evolution of the climate network and the HC, we further calculate the stream function (Eq. **8**; see ref. 37) as a function of time, and from this, we evaluate the changes in the meridional width ϕ_H and strength Ψ of the HC. We show the results in *SI Appendix*, Fig. S3 for the ERA-Interim reanalysis data and for a CMIP5 model under the RCP8.5 scenario; this model was chosen due to its relatively high *r* value. Similarly, we define ξ_{ϕ_H} and ξ_Ψ as the change rates (the slope of the trend line) for the width and intensity of the HC. Fig. 3 *D–F* shows the corresponding results, where, as previously reported (35, 36, 38), most of the CMIP5 models exhibit weakening and expansion of the HC (i.e., $\xi_\Psi < 0$, $\xi_{\phi_H} > 0$). *SI Appendix*, Fig. S4 depicts the results of a few CMIP5 models and indicates that there is a significant positive correlation between the tropical cluster intensity, W_c, and the intensity of the HC, Ψ. Similar correlations have also been observed between the width of the tropical cluster, G_c, and the width of the HC, ϕ_H, for each individual model. A similar significant positive relationship has been found across all models by comparing ξ_W and ξ_Ψ (Fig. 3 *G–I*). *SI Appendix*, Fig. S5 shows the positive relationship between the width of the tropical cluster and the HC. These results indicate that the tropical component of the climate network is correlated with the HC.

It should be noted that in contrast to model and theory (36, 38), an increasing trend is found in the strength of HC in ERA Interim (*SI Appendix*, Fig. S3*A*). This is also confirmed by other NCEP–NCAR and ERA-40 reanalysis datasets (39). A tentative hypothesis trying to resolve this contradiction was recently suggested (38). It is assumed that the increasing trends are artifacts related to the fact that the tropical lapse rate in the radiosonde data are increasing rather than staying close to a moist adiabat. However, researchers still have not found a way to deal with these artifacts. Our network–percolation approach seems to be more robust as it yields consistent decreasing trend strength for the different datasets, including models and reanalysis, as well as different time periods. This is most likely due to the fact that the network–percolation approach is based on surface temperature data only. *SI Appendix*, Fig. S6 shows our network results tested on the ERA-40 reanalysis—we find the same tendency of a weakening and an expansion of the tropical component under global warming.

Potential Effects and Practical Applications

The Intergovernmental Panel on Climate Change (IPCC) forecasts a temperature rise of 1.4 to 5.6 °C over this century (by 2100) (4). Here, we associate the HC circulation with the tropical component found by the network–percolation approach. The locations of the subtropical dry zones and the major tropical/subtropical deserts are associated with the subsiding branches of the HC (38, 40). Therefore, the poleward expansion of the HC may result in a drier future in some tropical/subtropical regions (35); the network–percolation analysis we propose here may help identify (to some degree) the regions that are more probable to experience decline in precipitation. Another potential effect is the poleward migration of the location of tropical cyclone maximum intensity (41); again, the method we propose may help (to some degree) to forecast these "high risk" regions. There is thus a great interest in clarifying/predicting the influenced climatological areas in response to global warming.

To identify the climate change response, for simplicity but without loss of generality, we compare, in Fig. 4, the topology of the tropical component for the first and last twenty years of the 21st century, i.e., 2080–2100 vs. 2006–2026. Counting the number of models that simulate these changes (Fig. 4), one can see that the overall pattern of stable node change is robust across most models; the patterns of adding nodes or removing nodes are shown in Fig. 4 *B* and *C*. We find that some regions, for example, northern India, southern Africa, and western Australia have a higher probability to be influenced by the tropical component (or HC), whereas the impacts in other regions, e.g., the Northeast Pacific, will become weaker in the future. We note that our method cannot detect the Fertile Crescent region that was shown to be one of the regions to dry significantly in the 21st century (42, 43). For ease of comparison, the datasets are interpolated into a $1^\circ \times 1^\circ$ longitude–latitude grid.

Discussion

As discussed above, although the conventional analysis of satellite observations and the climate change simulations of the IPCC Fourth Assessment Report project indicates a poleward expansion of the HC (33, 35), there are still two main unsolved issues. (*i*) The spatial (zonal) structure of this expansion is not fully resolved. (*ii*) In contrast to models and theoretical considerations (36, 38), which predict decreasing intensity of the HC, an increasing trend was found in the intensity of HC in reanalysis datasets

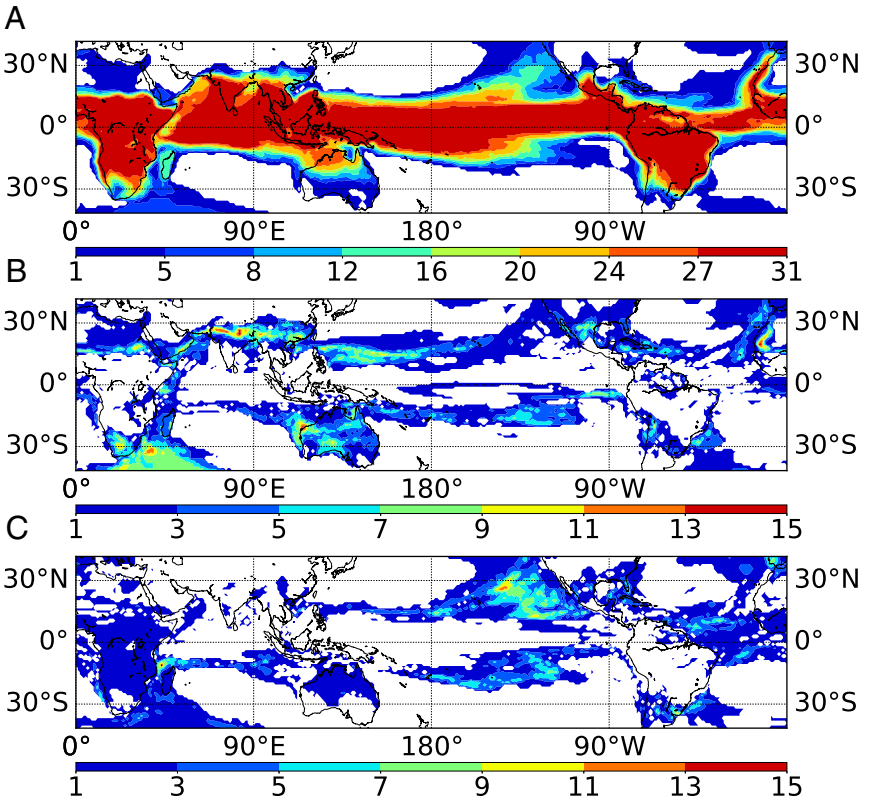

Fig. 4. The evolution of the largest (tropical) cluster under the RCP8.5 scenario for the 31 models. For each grid point (node), we compare the first and the last 20 y of the 21st century and show the number of models with stable nodes (i.e., nodes that were part of the topical cluster for both the first and the last 20 y of the 21st century) (*A*), added nodes (i.e., nodes that were part of the tropical cluster for the last 20 y of the 21st century but not for the first 20 y) (*B*), and removed nodes (i.e., nodes that were part of the tropical cluster for the first 20 y of the 21st century but not for the last 20 y) (*C*).

(39). Both issues can be resolved by the network–percolation approach we developed. (*i*) It provides both latitude and longitude evolution of the tropical component structure (Fig. 1*A*), and (*ii*) our approach exhibits a decreasing trend in the intensity of the HC in reanalysis datasets, as predicted by models and theory. This is probably since the network–percolation approach proposed here depends solely on the 2D surface temperature field, while the more conventional methods are based on the 3D (pressure levels) wind field.

In our report, the "abrupt" term is a concept from physical phase transitions and not necessarily related to abrupt (temporal) climate changes. It indicates discontinues or first-order phase transitions. It has been pointed out that a random network or lattice system always undergoes a continuous percolation phase transition and shows standard scaling features during a random process (25, 44). The question of whether percolation transitions could be discontinuous has attracted much attention recently in the context of interdependent networks (45) and the so-called explosive percolation models (46–48). Interestingly, the dynamic evolution of our climate network indicates the possibility of discontinuous phase transition, as shown in Fig. 1*B*. To further test the order of the percolation phase transitions, we study the finite size effects of our network by altering the resolution of nodes. The results are shown in *SI Appendix*, Fig. S7. It suggests a discontinuous percolation. For comparison, we also show the results for shuffled data (shuffled spatial), which exhibit a continuous phase transition. A first-order phase transition is abrupt and discontinuous, and a second order phase transition is a continuous transition (with a discontinuous derivative). In addition, an abrupt, first order, transition is much more "dangerous" than a continuous, second-order, one, since one failure is sufficient to completely disrupt the network. In that sense, the critical link with W_c is crucial and affects the whole climate with a shock.

In summary, we have used a network and percolation analysis on surface air temperature data and found that the largest (tropical) cluster expands poleward and experiences weakening under the influence of global warming. We show that these trends are significant, and we relate them to the weakening and poleward expansion of the HC atmospheric circulation. By comparing the topology of the tropical component for the first and last 20 y of the 21st century, i.e., 2080–2100 vs. 2006–2026, we clarify/predict the influenced climatological areas in response to global warming. Furthermore, we find an abrupt jump during the dynamical evolution of the climate network; using a finite size scaling analysis, we argue that the percolation transition is first order. The study of the climate system may enrich the understanding of the discontinuous phase transition. The proposed method and analysis provide a deep perspective on global warming and can potentially be used as a template to study other climate change phenomena.

Data and Methods

Data. In this study, we employ the monthly 2 m near-surface air temperature and 37 pressure level meridional wind velocity V of ERA-Interim (31) and ERA-40 (49) reanalysis datasets. The resolution is 0.125°, the time period spans from 1979 to 2016 for ERA-Interim and 1980 to 2005 for ERA-40. The data can be downloaded from apps.ecmwf.int/datasets.

For the climate projection, we used the RCP8.5, RCP4.5 and Historical scenarios of the CMIP5. RCP8.5 is the upper bound of the RCPs and does not include any specific climate mitigation target. The RCP8.5 assumes that greenhouse gas emissions and concentrations increase considerably over time, leading to a radiative forcing that will stabilize at about 8.5 Wm^{-2} at the end of the 21st century. All analyzed data are monthly mean surface air (2 m) temperatures and the meridional component of wind, V. The details of all 31 models we used are summarized in *SI Appendix*, Table S1. The data can be downloaded in pcmdi9.llnl.gov.

For each node i (i.e., longitude–latitude grid point), given a temperature record $\tilde{T}_i(t)$, where t stands for the month, we consider the month-to-month temperature difference

$$T_i(t) = \tilde{T}_i(t+1) - \tilde{T}_i(t). \quad [1]$$

We take the difference in Eq. **1** since we focus on climate change and how a change in one node affects other nodes; we repeated the analysis using the original time series and obtained similar clusters.

To obtain the strengths of the links between each pair of nodes i and j, we define the time-delayed, cross-correlation function as

$$C_{i,j}(\tau) = \frac{\langle T_i(t)\, T_j(t-\tau)\rangle - \langle T_i(t)\rangle \langle T_j(t-\tau)\rangle}{\sigma_{T_i(t)} \sigma_{T_j(t-\tau)}}, \quad [2]$$

and

$$C_{i,j}(-\tau) = C_{j,i}(\tau), \quad [3]$$

where $\sigma_{T_i(t)}$ is the SD (the square root) of $T_i(t)$, and τ is the time lag between 0 and 24 mo; for the networks that span a short time of 5 y, we set $\tau \in [0, 12]$. Eq. **2** is the definition for $\tau > 0$, while Eq. **3** is actually the definition for $\tau < 0$. Eq. **2** implicitly assumes that our process (the recordings of temperature T_i) is stationary, because the left-hand side only depends on the time lag, irrespective of the starting time t. We define the strength of the link as

$$W_{i,j} = \frac{\max(|C_{i,j}(\tau)|) - \mathrm{mean}(C_{i,j}(\tau))}{\mathrm{std}(C_{i,j}(\tau))}, \quad [4]$$

where "max", "mean," and "std" are the maximum, mean, and standard deviations of the cross-correlation (23). In the present work, we do not consider the direction but only the strength W_{ij} of each link. One should note that Eq. **2** is the time-delayed, cross-correlation function between two different nodes, and C_{ij} lies between -1 and 1. However, W_{ij} is calculated from C_{ij}, and its variations, and therefore according to Eq. **4**, can have values > 1.

Based on classic graph theory, a component is a subset of network nodes such that there exists at least one path from each node in the subset to another (14, 16). We denote $S_m(M)$ as a series of subnetworks; specifically, $S_1(M)$ indicates the largest cluster, $S_2(M)$ indicates the second largest cluster, and so forth, where M is the number of links (ordered by decreasing weight value) we added. In this study, due to the earth's spherical shape, the largest component in the climate networks is defined as

$$G_1(M) = \frac{\max\left[\sum_{i\in S_1(M)} \cos(\phi_i), \ldots, \sum_{i\in S_m(M)} \cos(\phi_i), \ldots,\right]}{\sum_{i=1}^{N} \cos(\phi_i)}, \quad [5]$$

where ϕ_i is the latitude of node i. Since our network is finite, we use the following procedure to determine the percolation threshold. We first calculate, during the growth process, the largest change of G_1 in Eq. **5**,

$$\Delta \equiv \max\left[G_1(2) - G_1(1), \ldots, G_1(M+1) - G_1(M), \cdots\right]. \quad [6]$$

The step with the largest jump in Eq. **6** is regarded as the phase transition point. We consider and analyze the weight of the critical link W_c and the size of the largest component G_c, which represent the intensity and size of the component. To measure the change of W_c and G_c within time, we anticipate the slope of the trend lines

$$W_c(t) = a + \xi_W * t$$
$$G_c(t) = b + \xi_G * t, \quad [7]$$

where ξ_W and ξ_G denote the increasing or decreasing trend rate, a and b are constants, and t is the time; we use a time interval of 5 y. We also performed a test for Fig. 2 and *SI Appendix*, Figs. S2–S6 by using exponential fit for W_c, G_c, Ψ, and ϕ and find that there are no significant differences (based on r values) between them. The reason for choosing linear fitting (Eq. **7**) is that in the conventional analysis, climate researchers found that the relationship of the change of HC and global warming (or time) follows linear scaling relations (not exponentially) (see refs. 34–36).

HC Index. The strength of the HC is computed using observed zonal-mean meridional wind in the stream function Ψ (37),

$$[\overline{V}] = \frac{g}{2\pi R \cos\phi}\frac{\partial \Psi}{\partial p}, \qquad [8]$$

where V is the meridional velocity in pressure coordinates, R is the mean radius of the earth, and p is the pressure. The operators $\bar{}$ and $[\,]$ stand for temporal and zonal averaging, respectively. We compute the Ψ field, assuming $\Psi = 0$ at the top of the atmosphere and integrating Eq. **8** downward to the surface. Since, in the winter, the HC is stronger, we only focus on the winter HC intensity. The analyses are performed on December–January–February (DJF) for the NH and June–July–August (JJA) for the SH separately. *SI Appendix*, Fig. S8 shows the mean stream function Ψ based on ERA-Interim during DJF and JJA.

Then we denote the maximum (minimum, respectively) of Ψ as Ψ_N (Ψ_S) during DJF (JJA) over the tropics $[-20°, 20°]$; the corresponding pressure level is denoted as p_N (p_S). The HC strength is defined as the difference between the values of the maximum and minimum, $\Psi = \Psi_N - \Psi_S$.

We identified the northern (southern) boundary ϕ_N (ϕ_S) of the HC as the first latitude north (south) poleward of Ψ_N (Ψ_S) at p_N (p_S) becomes zero. The poleward edges of the HC are defined as $\phi_H = \phi_N - \phi_S$. To measure the change of Ψ and ϕ_H within time, we define ξ_Ψ and ξ_{ϕ_H}, analogous to Eq. **7**.

ACKNOWLEDGMENTS. We thank Ori Adam and Maaian Rotstein at The Israeli Atmospheric and Climatic Data Center for helping to retrieve the CMIP5 data and Jianxi Gao, Daqing Li, and Xiaosong Chen for helpful discussions. We acknowledge the help in getting data of The Israeli Atmospheric and Climatic Data Center. We acknowledge the Israel–Italian collaborative project Network Aware Cyber Security, the Israel Science Foundation, Office of Naval Research, US Army Research Office, the Japan Science Foundation, Binational Science Foundation–National Science Foundation, and Defense Threat Reduction Agency (Grant HDTRA-1-10-1-0014) for financial support. J.F. and H.J.S. thank the "East Africa Peru India Climate Capacities" project, which is part of the International Climate Initiative. The Federal Ministry for the Environment, Nature Conservation and Nuclear Safety supports this initiative on the basis of a decision adopted by the German Bundestag. The Potsdam Institute for Climate Impact Research is leading the execution of the project, together with its project partners, The Energy and Resources Institute and the Deutscher Wetterdienst.

1. Schellnhuber HJ (2017) The 10 science 'must knows' on climate change, *23rd Conference of the Parties* (Future Earth, Stockholm). Available at www.futureearth.org/news/cop23-10-science-must-knows-climate-change. Accessed November 13, 2017.
2. Knutson TR, Kam J, Zeng F, Wittenberg AT (2018) Cmip5 model-based assessment of anthropogenic influence on record global warmth during 2016. *Bull Am Meteorol Soc* 99:S11–S15.
3. Gleick PH, et al. (2010) Climate change and the integrity of science. *Science* 328:689–690.
4. Pachauri RK, et al. (2014) *Climate Change 2014: Synthesis Report. Contribution of Working Groups I, II and III to the Fifth Assessment Report of the Intergovernmental Panel on Climate Change* (Intergovernmental Panel on Climate Change, Geneva). Available at www.ipcc.ch/report/ar5/syr. Accessed November 13, 2017.
5. Hsiang SM, Meng KC, Cane MA (2011) Civil conflicts are associated with the global climate. *Nature* 476:438–441.
6. Helbing D (2013) Globally networked risks and how to respond. *Nature* 497:51–59.
7. Schleussner CF, Donges JF, Donner RV, Schellnhuber HJ (2016) Armed-conflict risks enhanced by climate-related disasters in ethnically fractionalized countries. *Proc Natl Acad Sci USA* 113:9216–9221.
8. Carleton TA, Hsiang SM (2016) Social and economic impacts of climate. *Science* 353:aad9837.
9. Alpert P (2004) The water crisis in the e. mediterranean—and relation to global warming? *Water in the Middle East and in North Africa* (Springer, New York), pp 55–61.
10. Min SK, Zhang X, Zwiers FW, Hegerl GC (2011) Human contribution to more-intense precipitation extremes. *Nature* 470:378–381.
11. O'Gorman PA (2014) Contrasting responses of mean and extreme snowfall to climate change. *Nature* 512:416–418.
12. Caesar L, Rahmstorf S, Robinson A, Feulner G, Saba V (2018) Observed fingerprint of a weakening Atlantic Ocean overturning circulation. *Nature* 556:191–196.
13. Albert R, Barabási AL (2002) Statistical mechanics of complex networks. *Rev Mod Phys* 74:47–97.
14. Cohen R, Havlin S (2010) *Complex Networks: Structure, Robustness and Function* (Cambridge Univ Press, Cambridge, United Kingdom), pp 1–6.
15. Brockmann D, Helbing D (2013) The hidden geometry of complex, network-driven contagion phenomena. *Science* 342:1337–1342.
16. Newman M (2010) *Networks: An Introduction* (Oxford Univ Press, Oxford), pp 15–106.
17. Pastor-Satorras R, Castellano C, Van Mieghem P, Vespignani A (2015) Epidemic processes in complex networks. *Rev Mod Phys* 87:925–979.
18. Morone F, Makse HA (2015) Influence maximization in complex networks through optimal percolation. *Nature* 524:65–68.
19. Gómez-Gardeñes J, Soriano-Paños D, Arenas A (2017) Critical regimes driven by recurrent mobility patterns of reaction–diffusion processes in networks. *Nat Phys* 14:391–395.
20. Yamasaki K, Gozolchiani A, Havlin S (2008) Climate networks around the globe are significantly affected by el nino. *Phys Rev Lett* 100:228501.
21. Ludescher J, et al. (2013) Improved El Niño forecasting by cooperativity detection. *Proc Natl Acad Sci USA* 110:11742–11745.
22. Boers N, et al. (2014) Prediction of extreme floods in the eastern Central Andes based on a complex networks approach. *Nat Commun* 5:5199.
23. Fan J, Meng J, Ashkenazy Y, Havlin S, Schellnhuber HJ (2017) Network analysis reveals strongly localized impacts of El Niño. *Proc Natl Acad Sci USA* 114:7543–7548.
24. Meng J, Fan J, Ashkenazy Y, Bunde A, Havlin S (2018) Forecasting the magnitude and onset of el nino based on climate network. *New J Phys* 20:043036.
25. Bunde A, Havlin S, eds (1996) *Fractals and Disordered Systems* (Springer, New York), pp 115–170.
26. Cohen R, Erez K, ben Avraham D, Havlin S (2000) Resilience of the internet to random breakdowns. *Phys Rev Lett* 85:4626–4628.
27. Stauffer D, Aharony A (2003) *Introduction to Percolation Theory* (Taylor & Francis, Oxford), pp 60–68.
28. Taubert F, et al. (2018) Global patterns of tropical forest fragmentation. *Nature* 554:519–522.
29. Li D, et al. (2015) Percolation transition in dynamical traffic network with evolving critical bottlenecks. *Proc Natl Acad Sci USA* 112:669–672.
30. Meng J, Fan J, Ashkenazy Y, Havlin S (2017) Percolation framework to describe El Niño conditions. *Chaos An Interdiscip J Nonlinear Sci* 27:035807.
31. Dee DP, et al. (2011) The ERA-interim reanalysis: Configuration and performance of the data assimilation system. *QJR Meteorol Soc* 137:553–597.
32. Taylor KE, Stouffer RJ, Meehl GA (2012) An overview of cmip5 and the experiment design. *Bull Am Meteorol Soc* 93:485–498.
33. Fu Q, Johanson CM, Wallace JM, Reichler T (2006) Enhanced mid-latitude tropospheric warming in satellite measurements. *Science* 312:1179–1179.
34. Held IM, Hou AY (1980) Nonlinear axially symmetric circulations in a nearly inviscid atmosphere. *J Atmos Sci* 37:515–533.
35. Lu J, Vecchi GA, Reichler T (2007) Expansion of the Hadley cell under global warming. *Geophys Res Lett* 34:L06805.
36. Seo KH, Frierson DMW, Son JH (2014) A mechanism for future changes in Hadley circulation strength in CMIP5 climate change simulations. *Geophys Res Lett* 41:2014GL060868.
37. Vallis GK (2017) *Atmospheric and Oceanic Fluid Dynamics* (Cambridge Univ Press, Cambridge, United Kingdom), pp 485–541.
38. Held IM, Soden BJ (2006) Robust responses of the hydrological cycle to global warming. *J Clim* 19:5686–5699.
39. Mitas CM, Clement A (2005) Has the Hadley cell been strengthening in recent decades? *Geophys Res Lett* 32:L03809.
40. Kelley C, Ting M, Seager R, Kushnir Y (2012) The relative contributions of radiative forcing and internal climate variability to the late 20th Century winter drying of the Mediterranean region. *Clim Dyn* 38:2001–2015.
41. Kossin JP, Emanuel KA, Vecchi GA (2014) The poleward migration of the location of tropical cyclone maximum intensity. *Nature* 509:349–352.
42. Yatagai KA, Alpert P (2008) First super-high-resolution model projection that the ancient "Fertile Crescent" will disappear in this century. *Hydrolo Res Lett* 2:1–4.
43. Yatagai KA, Alpert P, Xie P (2008) Development of a daily gridded precipitation data set for the Middle East. *Adv Geosci* 12:165–170.
44. Bollobás B (2001) *Random Graphs* (Cambridge Univ Press, Cambridge, United Kingdom), pp 130–159.
45. Buldyrev SV, Parshani R, Paul G, Stanley HE, Havlin S (2010) Catastrophic cascade of failures in interdependent networks. *Nature* 464:1025–1028.
46. Achlioptas D, D'Souza RM, Spencer J (2009) Explosive percolation in random networks. *Science* 323:1453–1455.
47. Riordan O, Warnke L (2011) Explosive percolation is continuous. *Science* 333:322–324.
48. D'Souza RM, Nagler J (2015) Anomalous critical and supercritical phenomena in explosive percolation. *Nat Phys* 11:531–538.
49. Uppala SM, et al. (2005) The ERA-40 re-analysis. *Q J R Meteorol Soc* 131:2961–3012.